The Astrophysical Journal, 850:21 (7pp), 2017 November 20 https://doi.org/10.3847/1538-4357/aa9521

A Search for Low-energy Neutrinos Correlated with Gravitational Wave Events GW 150914, GW 151226, and GW 170104 with the Borexino Detector

M. Agostini[1], K. Altenmüller[2], S. Appel[2], V. Atroshchenko[3], Z. Bagdasarian[4], D. Basilico[5], G. Bellini[5], J. Benziger[6], D. Bick[7], G. Bonfini[8], D. Bravo[5,9], B. Caccianiga[5], F. Calaprice[10], A. Caminata[11], S. Caprioli[5], M. Carlini[8], P. Cavalcante[8,9], A. Chepurnov[12], K. Choi[13], D. D'Angelo[5], S. Davini[11], A. Derbin[14], X. F. Ding[1], A. Di Ludovico[10], L. Di Noto[11], I. Drachnev[1,14], K. Fomenko[15], A. Formozov[5,15,12], D. Franco[16], F. Froborg[10], F. Gabriele[8], C. Galbiati[10], C. Ghiano[11], M. Giammarchi[5], A. Goretti[10], M. Gromov[12], C. Hagner[7], T. Houdy[16], E. Hungerford[17], Aldo Ianni[8,27], Andrea Ianni[10], A. Jany[18], D. Jeschke[2], V. Kobychev[19], D. Korablev[15], G. Korga[17], D. Kryn[16], M. Laubenstein[8], E. Litvinovich[3,20], F. Lombardi[8,28], P. Lombardi[5], L. Ludhova[4,21], G. Lukyanchenko[3], L. Lukyanchenko[3], I. Machulin[3,20], G. Manuzio[11], S. Marcocci[1,11], J. Martyn[22], E. Meroni[5], M. Meyer[23], L. Miramonti[5], M. Misiaszek[18], V. Muratova[14], B. Neumair[2], L. Oberauer[2], B. Opitz[7], F. Ortica[24], M. Pallavicini[11], L. Papp[2], N. Pilipenko[14], A. Pocar[25], A. Porcelli[22], G. Ranucci[5], A. Razeto[8], A. Re[5], A. Romani[24], R. Roncin[8,16], N. Rossi[8], S. Schönert[2], D. Semenov[14], M. Skorokhvatov[3,20], O. Smirnov[15], A. Sotnikov[15], L. F. F. Stokes[8], Y. Suvorov[3,26], R. Tartaglia[8], G. Testera[11], J. Thurn[23], M. Toropova[3], E. Unzhakov[14], A. Vishneva[15], R. B. Vogelaar[9], F. von Feilitzsch[2], H. Wang[26], S. Weinz[22], M. Wojcik[18], M. Wurm[22], Z. Yokley[9], O. Zaimidoroga[15], S. Zavatarelli[11], K. Zuber[23], and G. Zuzel[18]
The Borexino Collaboration

[1] Gran Sasso Science Institute (INFN), I-67100 L'Aquila, Italy
[2] Physik-Department and Excellence Cluster Universe, Technische Universität München, D-85748 Garching, Germany
[3] National Research Centre Kurchatov Institute, 123182 Moscow, Russia
[4] IKP-2 Forschungzentrum Jülich, D-52428 Jülich, Germany
[5] Dipartimento di Fisica, Università degli Studi e INFN, I-20133 Milano, Italy
[6] Chemical Engineering Department, Princeton University, Princeton, NJ 08544, USA
[7] Institut für Experimentalphysik, Universität Hamburg, D-22761 Hamburg, Germany
[8] INFN Laboratori Nazionali del Gran Sasso, I-67010 Assergi (AQ), Italy
[9] Physics Department, Virginia Polytechnic Institute and State University, Blacksburg, VA 24061, USA
[10] Physics Department, Princeton University, Princeton, NJ 08544, USA
[11] Dipartimento di Fisica, Università degli Studi e INFN, I-16146 Genova, Italy
[12] Lomonosov Moscow State University Skobeltsyn Institute of Nuclear Physics, 119234 Moscow, Russia
[13] Department of Physics and Astronomy, University of Hawaii, Honolulu, HI 96822, USA
[14] St. Petersburg Nuclear Physics Institute NRC Kurchatov Institute, 188350 Gatchina, Russia
[15] Joint Institute for Nuclear Research, 141980 Dubna, Russia
[16] AstroParticule et Cosmologie, Université Paris Diderot, CNRS/IN2P3, CEA/IRFU, Observatoire de Paris, Sorbonne Paris Cité, F-75205 Paris Cedex 13, France
[17] Department of Physics, University of Houston, Houston, TX 77204, USA
[18] M. Smoluchowski Institute of Physics, Jagiellonian University, 30059 Krakow, Poland
[19] Kiev Institute for Nuclear Research, 03028 Kiev, Ukraine
[20] National Research Nuclear University MEPhI (Moscow Engineering Physics Institute), 115409 Moscow, Russia
[21] RWTH Aachen University, D-52062 Aachen, Germany
[22] Institute of Physics and Excellence Cluster PRISMA, Johannes Gutenberg-Universität Mainz, D-55099 Mainz, Germany
[23] Department of Physics, Technische Universität Dresden, D-01062 Dresden, Germany
[24] Dipartimento di Chimica, Biologia e Biotecnologie, Università degli Studi e INFN, I-06123 Perugia, Italy
[25] Amherst Center for Fundamental Interactions and Physics Department, University of Massachusetts, Amherst, MA 01003, USA
[26] Physics and Astronomy Department, University of California Los Angeles (UCLA), Los Angeles, California 90095, USA
Received 2017 July 12; revised 2017 October 18; accepted 2017 October 18; published 2017 November 14

Abstract

We present the results of a low-energy neutrino search using the Borexino detector in coincidence with the gravitational wave (GW) events GW 150914, GW 151226, and GW 170104. We searched for correlated neutrino events with visible energies greater than 250 keV within a time window of ±500 s centered around the GW detection time. A total of five candidates were found for all three GW events combined. This is consistent with the expected number of solar neutrino and background events. As a result, we have obtained the best current upper limits on all flavor neutrino (ν_e, ν_μ, ν_τ) fluence associated with GW events, in the neutrino energy range 0.5–5.0 MeV.

Key words: gravitational waves – neutrinos

1. Introduction

The observation of the two gravitational wave (GW) events GW 150914 and GW 151226 and the candidate LVT151012 by the LIGO experiment (Abbott et al. 2016a, 2016b, 2016c) triggered an intensive follow-up campaign with neutrino detectors (Aab et al. 2016; Abe et al. 2016; Adrián-Martínez et al. 2016; Gando et al. 2016). Cerenkov neutrino telecopes (ANTARES, IceCube; Adrián-Martínez et al. 2016) and the Pierre Auger Observatory (Aab et al. 2016) have searched for high-energy neutrinos above 100 GeV and 100 PeV, respectively. KamLAND has searched for inverse beta decay (IBD)

[27] Also at: Laboratorio Subterráneo de Canfranc, Paseo de los Ayerbe S/N, E-22880 Canfranc Estacion Huesca, Spain.
[28] Present address: Physics Department, University of California, San Diego, CA 92093, USA.

antineutrino events with energies in the range of 1.8–111 MeV (Gando et al. 2016), and Super-Kamiokande has reported their results for neutrino signals in the neutrino energy range from 3.5 MeV to 100 PeV (Abe et al. 2016). The neutrino and antineutrino events within a time window of ±500 s around the GW detection time were analyzed in the detectors mentioned above, but no evidence for an excess of coincident neutrino events was reported.

Electromagnetic detectors of photons, including X-rays and γ-rays (Ackermann et al. 2016; Diaz et al. 2016; Savchenko et al. 2016; Tavani et al. 2016; Troja et al. 2016; Racusin et al. 2017), also did not observe an excess covering various wavelengths of electromagnetic radiation, except the *Fermi*-gamma-ray burst monitor, which reported a weak excess above 50 keV and 0.4 s after GW 159014 (Connaughton et al. 2016; see, however, Greiner et al. 2016; Savchenko et al. 2016).

The combination of data from GW, neutrino, and electromagnetic detectors forms a new multimessenger approach that might lead to a more complete understanding of astrophysical and cosmological processes.

Recently the LIGO and Virgo Collaborations reported the observation of GW 170104, a GW signal measured on 2017 January 4 and produced by the coalescence of two black holes (BHs) with masses $31.2^{+8.4}_{-6.0}M_{\odot}$ and $19.4^{+5.3}_{-5.9}M_{\odot}$ (Abbott et al. 2017). Here we report the results of a search for signals with visible energies greater than 0.25 MeV in the Borexino detector in coincidence with GW 150914, GW 151226, and GW 170104 events. We look for neutrino signals from ν_e, $\nu_{x=\mu,\tau}$ and antineutrinos $\bar{\nu}_e$, $\bar{\nu}_{x=\mu,\tau}$ from GW events that scatter on electrons. We also search for signals of $\bar{\nu}_e$ that induce IBD on protons.

Using the unique features of the Borexino detector—outstanding low-level background, large scintillator mass, and low-energy threshold—new limits on low-energy neutrino fluence correlated with detected GW events have been obtained.

2. Borexino Detector

Borexino is a liquid scintillator detector located underground at 3400 m of water equivalent in the Gran Sasso Laboratory, Italy.

The detector design is based on a concept of graded shielding such that the radio purity level increases moving toward the detector center. The main housing of the detector is a cylinder with a hemispheric top with a diameter of 18 m and height of 15.7 m and is made of stainless steel with high radio purity. Contained inside is a stainless steel sphere (SSS) with a diameter of 6.75 m and thickness of 8 mm fixed in place by a stainless steel support structure. The space between the outer barrel and SSS is filled with ultrapure water and is equipped with 208 8-inch photomultiplier tubes (PMTs). It serves as a Cerenkov muon veto and is called the outer detector (OD). The inner side of the SSS is equipped with 2212 8-inch PMTs of the inner detector (ID), and the inner volume is filled with pseudocumene (C_9H_{12}). The ID contains two transparent spherical nylon vessels with a refractive index similar to that of pseudocumene with radii of 5.5 m (radon barrier) and 4.25 m (inner vessel [IV]) located concentrically within the SSS (see Figure 1). The nylon used for these vessels was produced underground to fulfill high radio purity requirements.

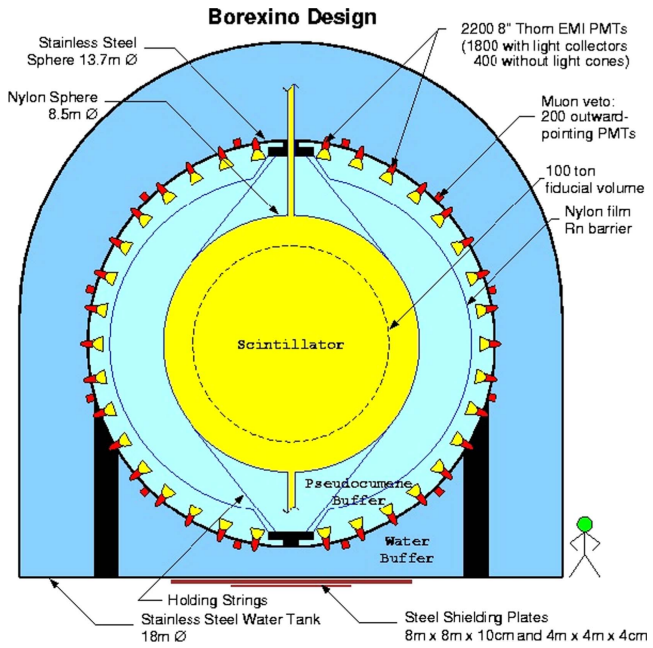

Figure 1. Principal scheme of the Borexino neutrino detector. Doping of PPO and DMP is shown in yellow and cyan, respectively. The fiducial volume is shown in an arbitrary way and does not reflect the one used in the current analysis.

The scintillator volume inside the IV has an admixture 1.5 g/l of PPO (2,5-diphenyloxazole, $C_{15}H_{11}NO$), which creates a Stokes shift (Stokes 1852). The scintillator outside the IV is doped with 2.8 g/l DMP (dimethylphthalate, $C_6H_4(COOCH_3)_2$), which quenches light production, decreasing scintillation signals whose origin is not in the IV.

The detector was carefully purified with various liquid handling procedures including water extraction campaigns and shows an exceptionally low level of radioactive impurities in the bulk of the IV fluid (Alimonti et al. 2009).

The energy and position of each event are reconstructed by exploiting the number of detected photons and their arrival times. The energy and position resolution (σ) are ≈50 keV and ≈10 cm at 1 MeV, respectively; both depend on the energy of the event as $\sim E^{-1/2}$. In contrast with water Cerenkov detectors, Borexino cannot retain directional information of the event, due to the isotropic emission of scintillation light.

Neutrinos of all flavors are detected by means of their elastic scattering of electrons:

$$\nu_{e,\nu,\tau} + e^- \rightarrow \nu_{e,\nu,\tau} + e^-. \quad (1)$$

In the scattering process, only a fraction of the neutrino energy E_ν is transferred to an electron, and the interaction of the latter with the medium creates the scintillation signal.

Electron antineutrinos ($\bar{\nu}_e$) are detected via the IBD process,

$$\bar{\nu}_e + p \rightarrow e^+ + n, \quad (2)$$

with a threshold of 1.806 MeV. The deposited $\bar{\nu}_e$ energy results in a prompt signal induced by the positron and includes the annihilation photons. The visible energy is related to the $\bar{\nu}_e$ energy as $E_{\rm vis} = E_\nu - 0.784$ MeV. A delayed signal induced by neutron capture on protons produces the 2.22 MeV gamma ray, providing a delayed coincidence signal with a mean capture time of 260 μs (Agostini et al. 2015b).

A detailed description of the detector can be found elsewhere (Alimonti et al. 2002, 2009; Bellini et al. 2014b).

Borexino first detected and then precisely measured the flux of the ^{7}Be solar neutrinos (Arpesella et al. 2008a, 2008b; Bellini et al. 2011b), has ruled out any significant day–night asymmetry of their interaction rate (Bellini et al. 2012a), has measured the ^{8}B-neutrino rate with a 3 MeV threshold (Bellini et al. 2010a), has made the first direct observation of pep neutrinos (Bellini et al. 2012c), has made the first spectral measurement of pp-neutrinos (Bellini et al. 2014a), and has set the best upper limit on the flux of solar neutrinos produced in the CNO cycle (Bellini et al. 2012c).

The unique, low background level of the Borexino detector made it possible to set new limits on the effective magnetic moment of the neutrino (Arpesella et al. 2008a; Agostini et al. 2017b), on the stability of the electron decay into a neutrino and a photon (Agostini et al. 2015a), on the heavy sterile neutrino mixing in ^{8}B decay (Bellini et al. 2013), on the possible violation of the Pauli exclusion principle (Bellini et al. 2010b), on the flux of high-energy solar axions (Bellini et al. 2012b), on antineutrinos from the Sun and other unknown sources (Bellini et al. 2011c), on gamma-ray burst neutrino and antineutrino fluences (Agostini et al. 2017a), and on some other rare processes.

3. Data Selection

The aim of data selection is to provide maximum exposure with minimum background contribution. Since the electron neutrino scattering searched in the current analysis has no interaction signature, it is important that backgrounds are reduced using knowledge of their characteristics. The following backgrounds are taken into consideration:

1. Short-lived cosmogenic backgrounds ($\tau \lesssim 1$ s) produced within the detector fiducial volume, such as ^{12}B, ^{8}He, ^{9}C, ^{9}Li, etc.
2. Other cosmogenic backgrounds, produced within the detector fiducial volume, such as ^{11}Be, ^{10}C, ^{11}C, etc.
3. Backgrounds of the inner nylon vessel, such as ^{210}Pb and uranium/thorium decay chains.
4. Natural backgrounds contained in the bulk of the detector fluid, such as ^{14}C, ^{85}Kr, ^{210}Bi, and ^{210}Pb.

These backgrounds can be suppressed by using ID/OD coincidences and position reconstruction. Cosmogenic backgrounds can be reduced by applying a temporal veto after each detected muon by pulse-shape discrimination (Bellini et al. 2011a). A veto length of 0.3 s after muons is applied to suppress ^{12}B to a statistically nonsignificant level and reduce ^{8}He, ^{9}C, and ^{9}Li by factor of 3 with a live-time loss of 1%.

Backgrounds contained in the bulk of the scintillator fluid cannot be avoided since they cannot be localized either spatially or temporally. Nevertheless, the number of counts can be reduced by setting a cut on the energy of events. This is important owing to the presence of ^{14}C in the scintillator. ^{14}C produces a beta spectrum with an endpoint of 0.156 MeV and has an activity of roughly 110 Bq in the whole IV.

The presence of this spectral component sets the lower threshold of the analysis to 0.25 MeV of visible energy.[29] An additional energy threshold of 0.4 MeV is also used to reduce the ^{210}Po and ^{210}Bi background decays and the ^{7}Be solar neutrino scattering on electrons.

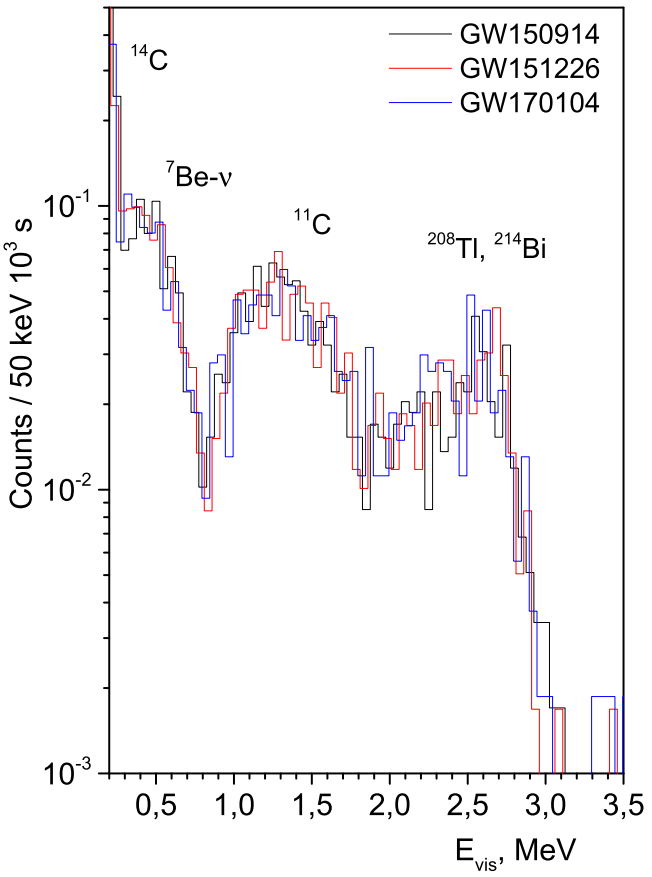

Figure 2. Energy spectrum of Borexino detector data passing the selection criteria, obtained using weekly runs containing events GW 150914, GW 151226, and GW 170104. The spectra corresponding to GW 151226 and GW 170104 are shifted to the left by 15 and 30 keV, respectively, for illustrative purposes. The plot shows the main spectral components, such as recoil electrons produced in elastic scattering of solar neutrinos from ^{7}Be, decays of cosmogenic ^{11}C, and external gamma events caused by decays of ^{214}Bi and ^{208}Tl outside the fiducial volume.

Backgrounds contained in the nylon of the IV cannot be removed by any kind of purification and are therefore of the order of 10^{2}–10^{3} times higher than within the bulk of the scintillator. The most critical components are ^{214}Bi and ^{208}Tl decays. These nuclides undergo β and $\beta + \gamma$ decay processes with a continuous spectrum overlapping with the region used by this analysis. The only way to overcome this kind of background is to perform a geometrical cut on events, selecting those within a fiducial volume. The fiducial volume is defined such that all events within and farther than 75 cm away from the IV are kept, which corresponds to 3 standard deviations of position reconstruction uncertainty at the lowest energy threshold. The corresponding fiducial volume has a mass of 145 t.

The energy spectra after applying these data selection cuts for the 3 weeks containing GW events are shown in Figure 2. The spectra are dominated by ^{14}C in the region below 0.25 MeV, by electron recoil from solar ^{7}Be neutrinos between 0.25 and 1.0 MeV, by cosmogenic ^{11}C in the 1.0–2.0 MeV region, and by external gamma quanta of ^{214}Bi and ^{208}Tl in the 2.0–3.0 MeV region. All these components cannot be

[29] The energy spectrum of ^{14}C is broadened up to this value owing to the detector energy resolution.

Table 1
Average Borexino Count Rate in 7-day Runs Containing the GW Events in Terms of Events per 1000 s Interval for Thresholds of 0.25 and 0.4 MeV

GW Event	Threshold (MeV)	Count Rate (eV/1000 s)	Detected Events
GW 150914	0.25/0.4	$2.07 \pm 0.06/1.68 \pm 0.06$	2/0
GW 151226	0.25/0.4	$2.15 \pm 0.06/1.72 \pm 0.06$	1/1
GW 170104	0.25/0.4	$2.28 \pm 0.07/1.72 \pm 0.06$	2/1

Note. The number of registered events inside the ±500 s interval is shown in the rightmost column.

significantly reduced by any available data selection techniques without serious exposure loss. The final background rates are given in Table 1.

4. Analysis and Results

The observations of GW 150914, GW 151226, and GW 170104 were made on 2015 September 14, 2015 December 26, and 2017 January 4, respectively, at times when the Borexino detector was taking data. The detection time and energy of Borexino events passing all data selection cuts in ±3000 s windows around GW 150914, GW 151226, and GW 170104 are shown in Figure 3.

A time window of ±500 s around the GW 150914, GW 151226, and GW 170104 detection times is applied for further analysis. This time window covers the possible delay of a neutrino that propagates slower than GW (for a claimed distance of $d \approx 440$ Mpc for GW 151226 [Abbott et al. 2016b] the delay reaches 440 s for a 0.5 MeV neutrino with 70 meV mass[30]), as well as a possible earlier emission of neutrinos in the case of BH–BH mergers (Baret et al. 2011). Moreover, the choice is consistent with the time window chosen in various works (Aab et al. 2016; Abe et al. 2016; Adrián-Martínez et al. 2016; Gando et al. 2016).

Two energy ranges are used in this analysis: the first is from 0.25 to 15 MeV, and the second is from 0.4 to 15 MeV. The lower threshold of 0.25 MeV allows us to register neutrinos with energy as low as 0.41 MeV via neutrino–electron elastic scattering.

Applying the selection cuts listed above leaves five candidates within the ±500 s search window around the detection time of GW 150914, GW 151226, and GW 170104 (Figure 3). The events nearest in time had energies of 0.267, 0.485, and 0.700 MeV and occurred 265, 291, and 270 s after GW 150914, GW 151226, and GW 170104, respectively. One should note that there are no extra events below 1 MeV within an extended window of ±1000 s, which exceeds the propagation and emission delays. A delay of 1000 s corresponds to a 70 meV neutrino that has traveled 990 Mpc (the distance from GW 170104 is 880 Mpc) with the minimal detectable energy of 0.41 MeV.

According to Borexino data from weekly runs containing the GW events, the number of solar neutrino and background events expected in each 1000 s time window is given in Table 1 for the energy intervals 0.25–15 MeV and 0.4–15 MeV, respectively. The

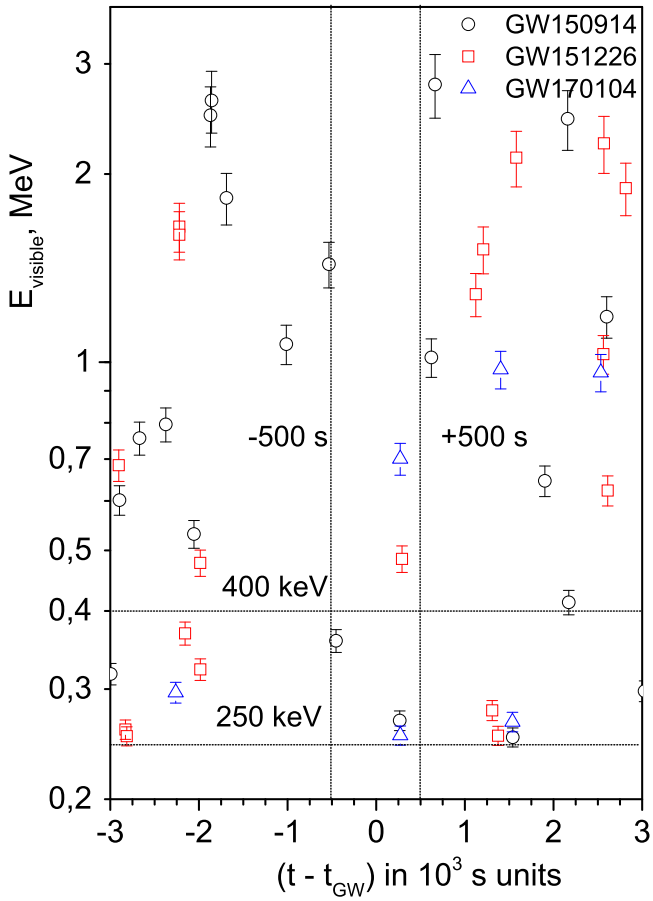

Figure 3. Borexino events with energy between 0.25 and 15 MeV occurring within ±3000 s of GW 150914 (black circles), GW 151226 (red squares), and GW 170104 (blue triangles) detection times. The closest events with energies 0.267, 0.485, and 0.700 MeV occurred at 265, 291, and 270 s after GW 150914, GW 151226, and GW 17010, respectively. All events are consistent with the expected solar neutrino and background count rate.

total number of solar neutrinos and background events expected for three 1000 s time windows is (6.5 ± 0.1) $(10^3$ s 145 t$)^{-1}$ and (5.1 ± 0.1) $(10^3$ s 145 t$)^{-1}$, respectively. These values should be compared with the total number of events detected during three 1000 s time windows in the corresponding energy interval (five and two events) $(10^3$ s 145 t$)^{-1}$. One can see that no excess of the counting rate, associated with GW events, above the expected background is observed.

The upper limits on the fluence for monoenergetic (anti) neutrinos with energy E_ν are calculated as follows:

$$\Phi = \frac{N_{90}(E_\nu, n_{\rm obs}, n_{\rm bkg})}{\epsilon N_e \sigma(E_{\rm th}, E_\nu)}, \quad (3)$$

where $N_{90}(E_\nu, n_{\rm obs}, n_{\rm bkg})$ is the 90% C.L. upper limit on the number of GW-correlated events in the $(E_{\rm th}, E_\nu)$ range per single GW event, ϵ is the recoil electron detection efficiency, $N_e = 4.79 \times 10^{31}$ is the number of electrons in the Borexino fiducial volume, $\sigma(E_{\rm th}, E_\nu)$ is the total neutrino–electron cross section integrated over the $(E_{\rm th}, E_\nu)$ interval. The recoil electron detection efficiency equals 1, with precision on the fiducial volume definition of 4%. The upper limit $N_{90}(E_\nu, n_{\rm obs}, n_{\rm bkg})$ is calculated for the total number of observed events during three 1000 s intervals ($n_{\rm obs} = 5$ for the 0.25 MeV threshold) and for the known mean background

[30] The *Planck* 2015 cosmic microwave background temperature and polarization power spectra in combination with the baryon acoustic oscillation data give a limit on the sum of neutrino masses $\sum m_\nu \leqslant 0.17$ eV at 95% C.L. (Planck Collaboration et al. 2016). Together with the measured oscillation mass differences (Patrignani et al. 2016), it leads to a constraint on the maximum neutrino mass m_1, m_2, m_3 of 70 meV.

Table 2
Upper Limits on Fluence per Single GW Event for All Neutrino Flavors in 10^{12} cm^{-2} Units at 90% C.L. Calculated for Monochromatic Neutrino Lines

E_ν (MeV)	ν_e	ν_x	$\bar{\nu}_e$	$\bar{\nu}_x$	$\bar{\nu}_e$ IBD
0.5	50	178	452	211	⋯
1.0	6.5	31	23	37	⋯
2.0	1.4	7.2	3.8	8.6	2.54
3.0	0.52	2.8	1.4	3.4	0.32
4.0	0.36	2.0	0.9	2.4	0.13
5.0	0.28	1.6	0.69	1.9	0.067

$n_{\rm bkg}$ in accordance with the procedure (Feldman & Cousins 1998), and then the limit was reduced per one GW event to compare different experiments. The total cross section $\sigma(E_{\rm th}, E_\nu)$ is obtained by integrating the (ν, e)-scattering cross section $d\sigma(E_\nu)/dE_e$ (Bahcall et al. 1995) over electron recoil energies E_e between the electron threshold energy $E_{\rm th}$ and the neutrino energy E_ν:

$$\sigma(E_{\rm th}, E_\nu) = \int \frac{d\sigma(E_\nu, E_e)}{dE_e} dE_e. \quad (4)$$

The limits obtained for various neutrino energies are summarized in Table 2. The obtained constraints are shown in Figure 4, along with the results from Super-Kamiokande (Abe et al. 2016). Borexino has set the best limits in the neutrino energy interval 0.5–5.0 MeV.

Since electron antineutrinos with energies greater than 1.8 MeV can interact with protons via IBD, we calculate their fluence upper limits for monoenergetic antineutrinos using relation (3) but replacing N_e with the number of protons N_p. The analysis is similar to a geo-neutrino search by Borexino based on $(5.5 \pm 0.3) \times 10^{31}$ protons × yr exposure. Only 77 antineutrino candidates were registered within 1842 live-time days of data taking (Agostini et al. 2015b). No IBD interactions were observed in ±500 s time windows around GW 150914, GW 151226, and GW 170104 where the expected background is close to zero, so the 90% C.L. upper limits on the number of GW-correlated events $N_{90}(E_\nu, n_{\rm obs}, n_{\rm bkg})$ is 2.44 (Feldman & Cousins 1998). The IBD cross section for antineutrinos was calculated according to Strumia & Vissani (2003). The results are shown in Figure 4, line 5 along with the limits from KamLAND (Gando et al. 2016), and in Table 2, sixth column.

If the neutrino spectrum $\phi(E_\nu)$ is not a monochromatic line, the total cross section for the electron recoil energy interval (E_1, E_2) required for Equation (3) is calculated as

$$\sigma(E_1, E_2) = \int\int \frac{d\sigma(E_\nu, E_e)}{dE_e} \phi(E_\nu) dE_e dE_\nu. \quad (5)$$

Since there is no reliable theory for the low-energy part of the neutrino emission spectrum for BH–BH mergers, we calculate the fluence limits for two variants of the neutrino spectrum $\phi(E_\nu)$. The first variant we considered was a standard power-law model. Since the neutrino energies that Borexino is sensitive to are relatively low, we drop the E^{-2} dependence that is expected for high-energy (>100 MeV) neutrinos and adopt the flat spectrum also used in (Abe et al. 2016). Additionally, we calculate the limits for the spectrum given by the normalized Fermi–Dirac (F–D) distribution for effective neutrino temperature T, connected to the average neutrino

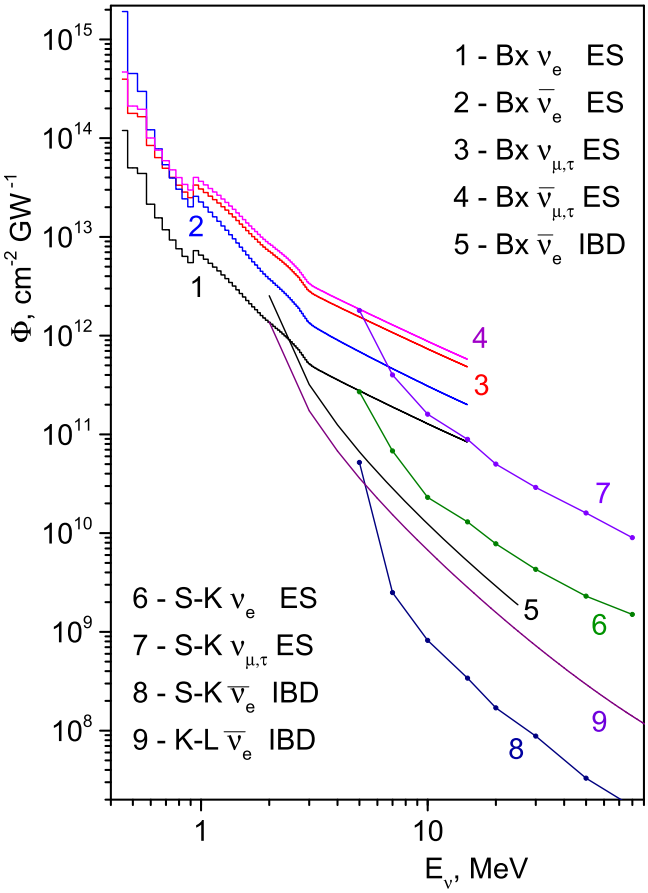

Figure 4. Borexino 90% C.L. fluence upper limits obtained by neutrino–electron elastic scattering for ν_e (line 1), $\bar{\nu}_e$ (line 2), $\nu_{\mu,\tau}$ (line 3), $\bar{\nu}_{\mu,\tau}$ (line 4), and through IBD for $\bar{\nu}_e$ (line 5). Given are also the limits obtained by Super-Kamiokande (lines 6, 7, 8) and KamLAND (line 9).

energy as $\langle E \rangle \simeq 3\ T$ and zero chemical potential ($\eta = 0$):

$$\phi(E_\nu, T) \propto \frac{(E_\nu)^2}{1 + \exp(E_\nu/T - \eta)}. \quad (6)$$

Although usage of the F–D distribution for approximation of the neutrino spectrum is only well motivated for a thermal neutrino flux (e.g., in the case of core-collapse supernovae; Janka & Hillebrandt 1989; Keil et al. 2003; Tamborra et al. 2012), whereas outflowing energy released during BH–BH mergers might produce nonthermal radiation, it could still have a similar neutrino component, e.g., in the case of neutrinos emitted from BH accretion disks (Caballero et al. 2012, 2016).

Substituting the flat normalized distribution for neutrino energies between 0 and 75 MeV ($\phi(E_\nu) = \text{const}$) into Equation (5) and integrating over the analyzed electron recoil energy interval $(E_1, E_2) = (0.4, 15.0)$ MeV, one gets the limits on the total electron neutrino fluence per single GW event:

$$\Phi(\nu_e) \leqslant 2.3 \times 10^{10}\ \text{cm}^{-2}. \quad (7)$$

Limits obtained for other neutrino flavors are shown in Table 3.

Limits on the fluence assuming an F–D distribution (Equation (6)) were obtained for different temperatures T within the energy range 0.5–30 MeV in steps of 0.5 MeV. This temperature range covers the neutrinos emitted by the explosion of supernovae or neutrinos from accretion disks around a BH (Caballero et al. 2012). The neutrino spectra were

Table 3
The 90% C.L. Upper Limits on GW Event Neutrino Fluence in 10^{11} cm^{-2} Units Assuming Two Different Neutrino Spectra

Spectrum	ν_e	ν_x	$\bar{\nu}_e$	$\bar{\nu}_x$	$\bar{\nu}_e$ IBD
Flat distribution	0.23	1.2	0.34	1.3	0.15
F–D ($T = 5$ MeV)	1.4	7.8	2.9	9.1	0.04

Note. Row 2: flat neutrino spectrum in the range 0–75 MeV; row 3: Fermi–Dirac spectrum for $T = 5$ MeV.

calculated for a wide energy interval of 0–500 MeV. The obtained limits are shown in Figure 5. The fluence constraints for the flat neutrino spectrum and F–D distribution with a temperature of 5 MeV are shown in Table 3. For comparison, the limit on the ν_e fluence in the case of a flat neutrino energy spectrum in the range 3.5–75 MeV is 1.2×10^9 cm^{-2} (Abe et al. 2016), and the limit on the $\bar{\nu}_e$ fluence for F–D neutrino spectra at $T = 4$ MeV is 3.6×10^9cm^{-2} (Gando et al. 2016).

The fluence upper limits can be converted into upper limits on the total energy radiated in the form of neutrinos for a BH–BH merger (E(BH–BH $\rightarrow \nu_{e,x}, \bar{\nu}_{e,x}$)).

Here, we consider only the energy radiated by electron neutrinos assuming a flat neutrino spectrum in the range 0–75 MeV and isotropic angular distribution. Usage of the LIGO-determined distance for GW 150914, GW 151226, and GW 170104 and relation (7) gives $E(\mathrm{BH}-\mathrm{BH} \rightarrow \nu_e) \leqslant 4.0 \times 10^{61}$ erg. This value can be compared with the energy emitted in the GW channel that is claimed to be around 2 solar masses per single GW, $2M_\odot = 3.6 \times 10^{54}$ erg. This suggests that successful detection of low-energy neutrinos should be possible only in the case of anisotropic angular distribution of neutrino emission. Limits on the energy radiated into neutrinos of other flavors can be easily calculated from Table 3.

5. Conclusion

We searched for an excess in the number of events detected by Borexino owing to neutrino–electron elastic scattering or IBD on protons correlated to the GW signals observed by the twin advanced LIGO interferometers. We found no statistically significant increase in the number of events, with a visible energy greater than 0.25 MeV in the detector during time windows of ±500 s around the GW 150914, GW 151226, and GW 170104 events. As a result, new limits on the fluence of monochromatic neutrinos of all flavors were set for neutrino energies in the range of 0.5–15 MeV. These are the strongest limits for $\nu_{e,\mu,\tau}$ and $\bar{\nu}_{\mu,\tau}$ for the neutrino energy range 0.5–5.0 MeV, and the constraint on electron antineutrino fluence based on ($\bar{\nu}_e$, e) scattering is the strongest in the 0.5–2.0 MeV energy range.

The Borexino program is made possible by funding from INFN (Italy); the NSF (U.S.); BMBF, DFG, HGF, and MPI (Germany); RFBR (grant nos. 15-02-02117, 16-29-13014, 16-02-01026, and 17-02-00305), RSF (grant no. 17-12-01009; Russia); NCN Poland (grant no. UMO-2013/10/E/ST2/00180); and FNP Poland (grant no. TEAM/2016-2/17). We acknowledge the generous support and hospitality of the Laboratori Nazionali del Gran Sasso (LNGS).

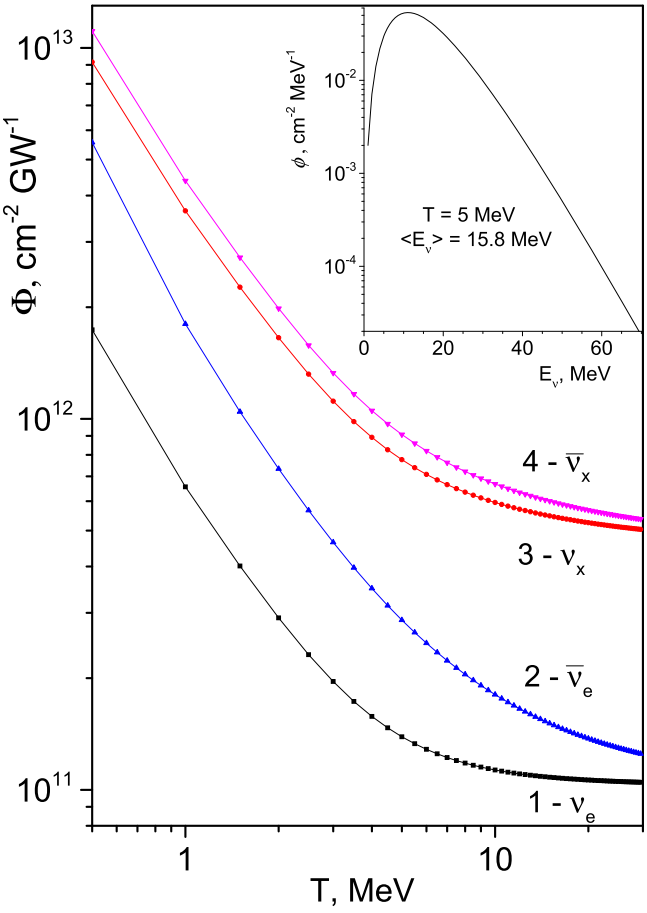

Figure 5. 90% C.L. upper limits on fluence for all neutrino flavors obtained using the F–D neutrino spectrum with respect to the effective neutrino temperature T. The inset shows the F–D neutrino spectrum for $T = 5$ MeV.

References

Aab, A., Abreu, P., Aglietta, M., et al. 2016, PhRvD, 94, 122007
Abbott, B. P., Abbott, R., Abbott, T. D., et al. 2016a, PhRvL, 116, 131103
Abbott, B. P., Abbott, R., Abbott, T. D., et al. 2016b, PhRvL, 116, 241103
Abbott, B. P., Abbott, R., Abbott, T. D., et al. 2016c, ApJL, 833, L1
Abbott, B. P., Abbott, R., Abbott, T. D., et al. 2017, PhRvL, 118, 221101
Abe, K., Haga, K., Hayato, Y., et al. 2016, ApJL, 830, L11
Ackermann, M., Ajello, M., Albert, A., et al. 2016, ApJL, 823, L2
Adrián-Martínez, S., Albert, A., André, M., et al. 2016, PhRvD, 93, 122010
Agostini, M., Altenmuller, K., Appel, S., et al. 2017a, APh, 86, 11
Agostini, M., Altenmüller, K., Appel, S., et al. 2017b, arXiv:1707.09355
Agostini, M., Appel, S., Bellini, G., et al. 2015a, PhRvL, 115, 231802
Agostini, M., Appel, S., Bellini, G., et al. 2015b, PhRvD, 92, 031101
Alimonti, G., Arpesella, C., Back, H., et al. 2002, APh, 16, 205
Alimonti, G., Arpesella, C., Back, H., et al. 2009, NIMPA, 600, 568
Arpesella, C., Back, H. O., Balata, M., et al. 2008a, PhRvL, 101, 091302
Arpesella, C., Bellini, G., Benziger, J., et al. 2008b, PhLB, 658, 101
Bahcall, J. N., Kamionkowski, M., & Sirlin, A. 1995, PhRvD, 51, 6146
Baret, B., Bartos, I., Bouhou, B., et al. 2011, APh, 35, 1
Bellini, G., Benziger, J., Bick, D., et al. 2011a, JInst, 6, P05005
Bellini, G., Benziger, J., Bick, D., et al. 2011b, PhRvL, 107, 141302
Bellini, G., Benziger, J., Bick, D., et al. 2012a, PhLB, 707
Bellini, G., Benziger, J., Bick, D., et al. 2012b PhRvD, 85, 092003
Bellini, G., Benziger, J., Bick, D., et al. 2012c PhRvL, 108, 051302
Bellini, G., Benziger, J., Bick, D., et al. 2013, PhRvD, 88, 072010
Bellini, G., Benziger, J., Bick, D., et al. 2014a Natur, 512, 383
Bellini, G., Benziger, J., Bick, D., et al. 2014b PhRvD, 89, 112007
Bellini, G., Benziger, J., Bonetti, S., et al. 2010a, PhRvD, 82, 033006
Bellini, G., Benziger, J., Bonetti, S., et al. 2011c, PhLB, 696, 191
Bellini, G., Bonetti, S., Buizza Avanzini, M., et al. 2010b, PhRvC, 81, 034317

Caballero, O. L., McLaughlin, G. C., & Surman, R. 2012, ApJ, 745, 170
Caballero, O. L., Zielinski, T., McLaughlin, G. C., & Surman, R. 2016, PhRvD, 93, 123015
Connaughton, V., Burns, E., Goldstein, A., et al. 2016, ApJL, 826, L6
Diaz, M. C., Beroiz, M., Peñuela, T., et al. 2016, ApJL, 828, L16
Feldman, G. J., & Cousins, R. D. 1998, PhRvD, 57, 3873
Gando, A., Gando, Y., Hachiya, T., et al. 2016, ApJL, 829, L34
Greiner, J., Burgess, J. M., Savchenko, V., & Yu, H. F. 2016, ApJL, 827, L38
Janka, H.-T., & Hillebrandt, W. 1989, A&A, 224, 49
Keil, M. T., Raffelt, G. G., & Janka, H.-T. 2003, ApJ, 590, 971
Patrignani, C., Agashe, K., Aielli, G., et al. 2016, ChPhC, C40, 100001
Planck Collaboration, Ade, P. A. R., Aghanim, N., et al. 2016, A&A, 594, A13
Racusin, J. L., Burns, E., Goldstein, A., et al. 2017, ApJ, 835, 82
Savchenko, V., Ferrigno, C., Mereghetti, S., et al. 2016, ApJL, 820, L36
Stokes, G. G. 1852, RSPT, 142, 463
Strumia, A., & Vissani, F. 2003, PhLB, 564, 42
Tamborra, I., Muller, B., Hudepohl, L., Janka, H.-T., & Raffelt, G. 2012, PhRvD, 86, 125031
Tavani, M., Pittori, C., Verrecchia, F., et al. 2016, ApJL, 825, L4
Troja, E., Read, A. M., Tiengo, A., & Salvaterra, R. 2016, ApJL, 822, L8